PHYSICAL REVIEW B **77**, 075425 (2008)

Atomistic calculations of interface elastic properties in noncoherent metallic bilayers

Changwen Mi, Sukky Jun,* and Demitris A. Kouris
Department of Mechanical Engineering, University of Wyoming, Laramie, Wyoming 82071, USA

Sung Youb Kim
Department of Mechanical Engineering, University of Colorado, Boulder, Colorado 80309, USA

(Received 21 August 2007; revised manuscript received 19 December 2007; published 26 February 2008)

The paper describes theoretical and computational studies associated with the interface elastic properties of noncoherent metallic bicrystals. Analytical forms of interface energy, interface stresses, and interface elastic constants are derived in terms of interatomic potential functions. Embedded-atom method potentials are then incorporated into the model to compute these excess thermodynamics variables, using energy minimization in a parallel computing environment. The proposed model is validated by calculating surface thermodynamic variables and comparing them with preexisting data. Next, the interface elastic properties of several fcc-fcc bicrystals are computed. The excess energies and stresses of interfaces are smaller than those on free surfaces of the same crystal orientations. In addition, no negative values of interface stresses are observed. Current results can be applied to various heterogeneous materials where interfaces assume a prominent role in the systems' mechanical behavior.

DOI: 10.1103/PhysRevB.77.075425 PACS number(s): 68.35.−p, 62.20.D−, 05.70.Np, 81.05.Bx

I. INTRODUCTION

Based on Eshelby's elasticity solution for an inclusion in an infinite medium,[1] continuum micromechanics has been used successfully to predict the mechanical properties of heterogeneous materials such as composites.[2,3] In recent years, with the advent of nanotechnology, a series of efforts has been made to extend this theoretical framework of continuum micromechanics to even smaller systems in which the characteristic length scales down to the order of tens of nanometers. In these studies, the significance of interface (or surface) effect is well recognized due to the high surface-to-volume ratio of the embedded nanoscale inclusion. Therefore, the major focus is directed toward incorporating interface effects into the theoretical framework of micromechanics. To list only a few examples, Cahn and Larché[4] examined the impact of interface stress on the mechanical and chemical equilibria of a small solid precipitate embedded in an infinite matrix of a different phase. Sharma *et al.*[5] revisited the same problem and, using a variational formulation, derived closed-form expressions for the elastic state. More recently, Mi and Kouris[6] extended this study from an infinite matrix to a semi-infinite substrate. In these studies, among several others, the classical theory of elasticity is modified especially in the vicinity of the boundary between the nanoparticle and the matrix medium in order to properly reflect surface and/or interface effects, and consequently results in a size-dependent stress state.

These continuum nanomechanics theories, though details vary, are typically formulated on the basis of the pioneering work by Gurtin and Murdoch,[7,8] who proposed the nonclassical stress-strain relationship featuring surface and/or interface effects. This constitutive equation consists of the surface and/or interface elastic moduli (for example, surface and /or interface Lamé constants, μ^S and λ^S as denoted in Ref. 5 under the isotropy assumption) in addition to other conventional constitutive terms. Therefore, the accurate determination of surface and/or interface elastic constants is of significant importance to practical applications of continuum nanomechanics theories for diverse nanoscale systems and materials. In contrast to their bulk counterparts, the surface and/or interface elastic moduli are not only intrinsic with the lattice structure considered but also variant depending upon surface and/or interface orientations and in-plane symmetries. Accuracy must be consistent with the atomic resolution, which makes experimental determination extremely difficult and is perhaps one of the reasons why, to the best of our knowledge, rigorous measurements of interface moduli have not been reported so far.

The atomistic computation of surface energy and surface stress has been so advanced that one of the most recent studies enabled the systematic investigation of the effect of surface defects on surface stresses of fcc metals.[9] There have also been several atomistic studies devoted to the computational determination of surface elastic constants of crystalline materials.[10–14] However, when it comes to bicrystal interfaces, only limited number of studies have been reported on the atomistic calculations of interface energy and interface stress.[15,16] Furthermore, no *interface elastic modulus tensor* has ever been considered rigorously by atomistic simulations; this fact motivated the current study.

In this paper, we present a systematic approach to the atomistic determination of interface elastic constants as well as interface energy and interface stress for various bicrystalline material systems. It is noted that our focus in this work is directed toward noncoherent interfaces only, similar to the work of Gumbsch and Daw.[15] We believe that there have been numerous *ab initio* and atomistic studies on the mechanical properties of epitaxially coherent interfaces. This is not within the scope of our current study, because the primary purpose of this paper is to provide the values of interface elastic constants, so that continuum nanomechanics is readily applicable to various heterogeneous nanostructures and nanocomposites containing noncoherent interfaces.

This paper is organized as follows. We first review briefly in Sec. II the derivation of surface and/or interface stresses

from thermodynamics. In Sec. III, we develop the analytical formulation of surface and/or interface modulus tensors with respect to elastic strains, based on the thermodynamic models of surface and interface. The general formulation is then implemented into the schemes of atomistic computer simulations in Sec. IV, which provides direct access to the surface and interface quantities in terms of empirical interatomic potential functions for metals. Simulation results are presented in Sec. V for several low-Miller-index fcc and bcc crystalline surfaces and interfaces. The discussion on these numerical results is also examined therein. Finally, concluding remarks are presented in Sec. VI.

II. REVIEW OF THERMODYNAMIC DEFINITIONS

While surface (interface) energy is defined as the energy cost to create a new surface (interface), the energy cost to deform a surface (interface) is represented by the surface (interface) stress.[17] In thermodynamics, the surface stress f is associated with the reversible work per unit area required to elastically strain a solid surface, at constant temperature.[18] In contrast to a fluid surface, the number of atoms per unit area or the electronic density of a solid surface do change under elastic strains. In order to account for this feature uniquely associated with solid surfaces, an extra term, in addition to the surface free energy density γ, must be included in the definition of surface stress[18] as

$$f_{\alpha\beta} = \frac{1}{A}\frac{\partial(\gamma A)}{\partial \epsilon_{\alpha\beta}} = \gamma\delta_{\alpha\beta} + \frac{\partial\gamma}{\partial\epsilon_{\alpha\beta}}, \tag{1}$$

where A defines the total surface area, $\delta_{\alpha\beta}$ denotes the Kronecker delta, and $\epsilon_{\alpha\beta}$ represents the in-plane strain tensor. By convention, the Greek subscripts refer to the surface-related quantities and assume values from 1 to 2. For a liquid surface, the surface stress is reduced to the second-order isotropic tensor of which the diagonal components equal to the surface free energy density. That is, the partial derivative in the last term of Eq. (1) vanishes. More details on surface stress can be found elsewhere such as the review articles by Cammarata[18] and Ibach.[19]

In a manner analogous to surface energy, the interface energy σ of an interface separating two single crystals is interpreted as the total excess energy possessed by all atoms close to the interface of interest, normalized by the interface area. Equivalently, this quantity defines the total work per unit area required to form a new interface. The term "excess" may be easily interpreted by a comparison between the particles residing in the interface region and those present in a perfect monocrystalline solid, under the same level of strain. Similar to the definition of surface stress, interface stress h characterizes the unit reversible work involved in deforming a preexisting interface. In principle, these two interface quantities can be measured through the diagram of reversible processes, as illustrated in Fig. 1.

Two reversible paths lead the initial state (illustrated in the upper left) to the identical final state (the lower right). In Path 1-to-2, the bicrystalline system with an initial interface area A under zero strain is first cleft into two monocrystals, and subsequently they are subjected to the same amount of infinitesimal strain $d\epsilon$. In the first step, the interface is traded for two surfaces of different single crystals as a result of the cleavage. The internal energy change associated with this process is

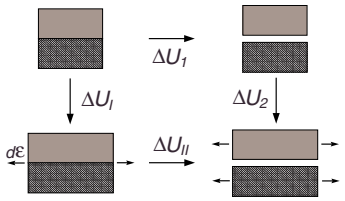

FIG. 1. (Color online) Reversible paths from which the relationship between interface energy and interface stress for an idealized bicrystalline interface can be derived.

$$\Delta U_1 = (\gamma^1 + \gamma^2 - \sigma)A, \tag{2}$$

where γ^1 and γ^2 denote, respectively, the surface free energy density of the two single crystals. Its sign depends on the competition between the original interface and the resultant two surfaces. The posterior deformation procedure involves work done against forces associated both with two surface stresses and with the classical volumetric ones. The second step of this path causes the energy change as

$$\Delta U_2 = A(f^1_{\alpha\beta} + f^2_{\alpha\beta})d\epsilon_{\alpha\beta} + \Delta U_B, \tag{3}$$

where ΔU_B denotes the change in bulk elastic energy. The summation convention is applied over the repeated Greek indices.

In the Path I-to-II, we perform the same separating and stretching procedures but in reverse order. During the first step, the work is done against the interface stress as well as against the bulk stresses within both single phases, which is given as

$$\Delta U_I = Ah_{\alpha\beta}d\epsilon_{\alpha\beta} + \Delta U_B. \tag{4}$$

The energy change corresponding to separating the strained bicrystal (the lower left in Fig. 1) is related to Eq. (2) by a differentiation in the energy densities and in the area as

$$\Delta U_{\mathrm{II}} = (\gamma^1 + d\gamma^1 + \gamma^2 + d\gamma^2 - \sigma - d\sigma)(A + dA). \tag{5}$$

On the other hand, both changes in bulk elastic energies (ΔU_B) during the second step of Path 1-to-2 and during the first step of Path I-to-II are equal. Therefore, the total energy difference between them corresponds to the work carried out against the interface stress $h_{\alpha\beta}$ subtracted by the one done against the two single crystal surface stresses $f^1_{\alpha\beta}$ and $f^2_{\alpha\beta}$ as

$$\Delta U_2 - \Delta U_I = A(f^1_{\alpha\beta} + f^2_{\alpha\beta} - h_{\alpha\beta})d\epsilon_{\alpha\beta}. \tag{6}$$

Finally, the path independence of the thermodynamics process depicted in Fig. 1 allows us to equate the total energy changes along both paths. With the help of Eqs. (2), (5), and (6), we thus have

$$d\{A(\gamma^1 + \gamma^2 - \sigma)\} = A(f^1_{\alpha\beta} + f^2_{\alpha\beta} - h_{\alpha\beta})d\epsilon_{\alpha\beta}, \tag{7}$$

where the higher-order terms involving the product of two differential quantities are omitted. In view of Eq. (1), an

analogy for an interface separating two inhomogeneous crystals can readily be obtained

$$h_{\alpha\beta} = \frac{1}{A}\frac{\partial(\sigma A)}{\partial \epsilon_{\alpha\beta}} = \sigma\delta_{\alpha\beta} + \frac{\partial\sigma}{\partial\epsilon_{\alpha\beta}}. \tag{8}$$

Equations (1) and (8) describe the thermodynamical definitions of surface and interface stresses, respectively. The two equalities in each equation imply two distinctive methods that we may use for practical calculations of $f_{\alpha\beta}$ and $h_{\alpha\beta}$. In the first equality, we concentrate on the strain derivative of total surface and/or interface energy normalized by the surface and/or interface area. In the second approach, the surface or interface energy density per unit area is first determined for each strain state. A finite difference scheme over several successive strains is then employed to extract the desired excess stresses. The computational cost associated with multiple strain states is generally still affordable for the determination of surface stress. However, as far as interface stresses and interface elastic constants are concerned, the cost becomes extremely high, mainly due to the following two reasons. First, the implementation of the in-plane periodic boundary conditions for a bicrystalline superlattice demands a huge supercell in order to avoid a relatively large residual mismatch strain in a noncoherent bilayer system.[15,16] The situation may get even worse due to the requirement of a large number of deformation levels for a full determination of all in-plane components of a modulus tensor.[12,14] The first method is hence computationally more preferable. Based on this approach, Ackland and Finnis[11] has successfully derived an analytical formulation in terms of the embedded atom method (EAM) potentials, in which only a single strain state was needed for $f_{\alpha\beta}$ or $h_{\alpha\beta}$. In the next section, we aim to extend such a computationally less expensive approach further to the atomistic determinations of interface elastic modulus tensor.

III. DERIVATION OF INTERFACE ELASTIC CONSTANTS

Assuming small deformations, the interface stress can be written using the Taylor series expansion around the zero-strain state as

$$h_{\alpha\beta}(\epsilon_{\mu\nu}) = (h_{\alpha\beta})_0 + \left(\frac{\partial h_{\alpha\beta}}{\partial \epsilon_{\mu\nu}}\right)_0 \epsilon_{\mu\nu} + \left(\frac{\partial^2 h_{\alpha\beta}}{\partial\epsilon_{\mu\nu}\partial\epsilon_{\delta\gamma}}\right)_0 \epsilon_{\mu\nu}\epsilon_{\delta\gamma} + \cdots, \tag{9}$$

where the subscript zero denotes that the evaluations are performed at zero-strain state. It is noted that the temperature and the remaining components of strain are held constant for the evaluation of a given partial derivative in Eq. (9). For small elastic strains, higher-order terms can be neglected. Following the linear strain assumption, this expansion results in a generalized interface constitutive equation as

$$h_{\alpha\beta}(\epsilon_{\mu\nu}) = (h_{\alpha\beta})_0 + c_{\alpha\beta\mu\nu}\epsilon_{\mu\nu}, \tag{10}$$

where the fourth-order interface elastic tensor is defined as the strain derivative of interface stress evaluated at the zero-strain configuration as

$$c_{\alpha\beta\mu\nu} = \left(\frac{\partial h_{\alpha\beta}}{\partial\epsilon_{\mu\nu}}\right)_0. \tag{11}$$

Even though Eq. (10) is of the same form as the classical constitutive equation of a linearly elastic bulk solid, its physical implication is different. For an isothermal bulk solid, zero strain corresponds to zero stress, so that there is no residual stress when the solid is free of deformation. However, a nonvanishing residual in-plane stress, $(f_{\alpha\beta})_0$ or $(h_{\alpha\beta})_0$, is generally present in isothermally bounded lattice structures even under zero strain.[12,18,19] As we shall see in the subsequent development, such an extra term results in additional loss of symmetries of the in-plane modulus tensor.

We express the interface constitutive behavior, Eq. (11), in terms of the internal energy state which is the total interface energy (σA) at zero temperature in this case. Both the interface energy density and the interface area are functions of applied strain. Taking the strain derivative over the first identity of Eq. (8), and noting that under homogeneous deformation the area change is dictated by

$$dA = Ad\epsilon_{\alpha\beta}\delta_{\alpha\beta}, \tag{12}$$

the interface elastic tensor in Eq. (11) can be rewritten as

$$c_{\alpha\beta\mu\nu} = \left\{\frac{1}{A}\frac{\partial^2(\sigma A)}{\partial\epsilon_{\alpha\beta}\partial\epsilon_{\mu\nu}} - \frac{1}{A}\frac{\partial(\sigma A)}{\partial\epsilon_{\alpha\beta}}\delta_{\mu\nu}\right\}_0. \tag{13}$$

Employing the definition of interface stress, this equation can be reformulated as

$$c_{\alpha\beta\mu\nu} = \left\{\frac{1}{A}\frac{\partial^2(\sigma A)}{\partial\epsilon_{\alpha\beta}\partial\epsilon_{\mu\nu}} - h_{\alpha\beta}\delta_{\mu\nu}\right\}_0, \tag{14}$$

in terms of the second-order internal energy derivative and the interface stress tensor.

Such a fourth-order elastic modulus tensor is quite formidable, since there are 16 components relating interface stress to the in-plane strain. Fortunately, even for the most anisotropic crystalline interface, symmetry arguments reduce the number of independent constants down to a maximum of nine. This reduction is enabled by the fact that $c_{\alpha\beta\mu\nu}$ is symmetric in α, β and μ, ν because $h_{\alpha\beta}$, $\epsilon_{\alpha\beta}$, and $\delta_{\alpha\beta}$ are symmetric second-order tensors. Unlike the bulk elastic tensor, no further reduction can be made by interchanging the pair of indices (α,β) with (μ,ν) due to the presence of the second term on the right hand side of Eq. (14). Additional symmetries in certain crystalline interfaces can also reduce the number of independent material constants further. For example, only five elastic components are independent for an interface separating two bcc crystals with (110) surface orientation. The crystalline interface structures of major interest is the one of a threefold (or higher) in-plane rotational symmetry. (111) fcc bicrystal and (0001) hcp bicrystal contain the interface of sixfold symmetry, and the interface made of two fcc (001) surfaces or two (001) bcc surfaces has fourfold symmetry. For these least anisotropic interfaces, the elastic modulus tensor is reduced to a general fourth-order isotropic tensor, in which only three components are independent.

Consequently, the interface stresses defined on such interfaces are simplified to a 2×2 isotropic tensor with equal normal and zero shear components.[20]

IV. IMPLEMENTATION OF EMPIRICAL POTENTIALS

Having the analytical forms of interface stress and interface elastic modulus, we implement selected empirical interatomic potentials into Eqs. (8) and (14) for atomistic calculations. We simulate the interatomic interaction using the EAM potentials developed by Johnson[21,22] for fcc and by Johnson and Oh[23] for bcc metals. For the purpose of validation, we also employ a simple empirical multibody potential proposed by Finnis and Sinclair[24] for bcc metals, which is based on the second-moment approximation to tight-binding theory (TB-SMA). The EAM and TB-SMA share a common mathematical form of interatomic interactions. That is, the total energy of a system of particles is expressed by

$$E_{tot}=\sum_i\left\{F_i(\rho_i)+\frac{1}{2}\sum_{j\neq i}\phi_{ij}(r_{ij})\right\}, \tag{15}$$

where ϕ_{ij} is the conventional pairwise potential term given as a function of the separation distance r_{ij} between atoms i and j.[21] $F_i(\rho_i)$ is the energy required to embed an atom at site i with a background electron density ρ_i, in which ρ_i is the sum over the atomic electron densities f_j due to all atoms interacting with i as

$$\rho_i=\sum_{j\neq i}f_j(r_{ij}). \tag{16}$$

The Roman subscripts refer to atoms throughout this paper and no summation should be assumed when repeated.

To integrate the interface stress and interface elastic tensor, i.e., Eqs. (8) and (14), the derivatives of potential functions have to be written in terms of strain. It has been shown that for a homogeneous deformation, the strain derivatives can be connected to the atomic coordinate gradient as follows:[11,25]

$$\frac{\partial}{\partial\epsilon_{\alpha\beta}}=\sum_{j\neq i}r_{ij\beta}\frac{\partial}{\partial r_{i\alpha}}\quad\text{and}\quad\frac{\partial^2}{\partial\epsilon_{\alpha\beta}\partial\epsilon_{\mu\nu}}=\sum_{j\neq i}r_{ij\beta}r_{ij\nu}\frac{\partial^2}{\partial r_{i\alpha}\partial r_{i\mu}}, \tag{17}$$

where $r_{ij\beta}$ and $r_{ij\nu}$, respectively, denote the β and ν components of the distance vector $\mathbf{r}_{ij}$. After tedious mathematical derivations, which are not presented here, we provide the final expressions for the interface energy, the interface stress tensor, and the interface modulus tensor in terms of EAM potentials, respectively, as follows.

In interface energy,

$$\sigma=\frac{1}{A}\sum_i(E_i-E_0),\quad E_i=F_i+\frac{1}{2}\sum_{j\neq i}\phi_{ij}. \tag{18}$$

In interface stress tensor,

$$h_{\alpha\beta}=\frac{1}{A}\sum_i\frac{\partial(E_i-E_0)}{\partial\epsilon_{\alpha\beta}},$$

$$\frac{\partial E_i}{\partial\epsilon_{\alpha\beta}}=\sum_{j\neq i}\left\{\frac{dF_i}{d\rho_i}\frac{df_j}{dr_{ij}}+\frac{1}{2}\frac{d\phi_{ij}}{dr_{ij}}\right\}\frac{r_{ij\alpha}r_{ij\beta}}{r_{ij}}. \tag{19}$$

In interface modulus tensor,

$$c_{\alpha\beta\mu\nu}=\frac{1}{A}\sum_i\left\{\frac{\partial^2(E_i-E_0)}{\partial\epsilon_{\alpha\beta}\partial\epsilon_{\mu\nu}}-\frac{\partial(E_i-E_0)}{\partial\epsilon_{\alpha\beta}}\delta_{\mu\nu}\right\},$$

$$\frac{\partial^2E_i}{\partial\epsilon_{\alpha\beta}\partial\epsilon_{\mu\nu}}-\frac{\partial E_i}{\partial\epsilon_{\alpha\beta}}\delta_{\mu\nu}=\frac{d^2F_i}{d\rho_i^2}\left(\sum_{j\neq i}\frac{r_{ij\alpha}r_{ij\beta}}{r_{ij}}\frac{df_j}{dr_{ij}}\right)\left(\sum_{j\neq i}\frac{r_{ij\mu}r_{ij\nu}}{r_{ij}}\frac{df_j}{dr_{ij}}\right)+\sum_{j\neq i}\left\{\frac{dF_i}{d\rho_i}\left(\frac{d^2f_j}{dr_{ij}^2}-\frac{1}{r_{ij}}\frac{df_j}{dr_{ij}}\right)+\frac{1}{2}\left(\frac{d^2\phi_{ij}}{dr_{ij}^2}-\frac{1}{r_{ij}}\frac{d\phi_{ij}}{dr_{ij}}\right)\right\}$$
$$\times\frac{r_{ij\alpha}r_{ij\beta}r_{ij\mu}r_{ij\nu}}{r_{ij}^2}+\sum_{j\neq i}\left\{\frac{dF_i}{d\rho_i}\frac{df_j}{dr_{ij}}+\frac{1}{2}\frac{d\phi_{ij}}{dr_{ij}}\right\}\frac{(\delta_{\alpha\mu}r_{ij\nu}-\delta_{\mu\nu}r_{ij\alpha})r_{ij\beta}}{r_{ij}}, \tag{20}$$

where E_i is the energy of an atom within an interface region and E_0 is the reference energy of an atom of the same species located in an infinite bulk crystal that is strained by the same amount. For an infinite monocrystal without any deformation, E_0 is simply equal to the negative cohesive energy per atom. Equation (19) is identical to the formula of interface stress in Ref. 15, since they used the same EAM-type potential functions for the calculation of interface stresses.

In the above equations, the determination of σ, $h_{\alpha\beta}$, and $c_{\alpha\beta\mu\nu}$ assumes a triple summation over atoms. The summation index i is limited to atoms on a single layer while the index j runs over all particles that are within an interacting distance from atom i. In addition, an extra summation is implemented over atomic layers with nonzero parameters of interest. Physically, the disturbance due to the presence of crystalline boundaries is responsible to these nonzero excess quantities. Under a homogeneous deformation, all atoms of an infinitely extended perfect monocrystal are equivalent. The equilibrium condition for such a lattice with energy functions given in Eq. (15) requires that the first-order strain

derivative of the total energy evaluated at zero-strain state vanishes, i.e., $(\partial E_{tot}/\partial \epsilon_{\alpha\beta})_0=0$. For bounded lattice structures, such as films and multilayers, however, this condition is violated due to the imperfection of chemical bonds close to crystalline boundaries. This nonvanishing first-order strain derivative, as shown in Eq. (19), serves as the source of the interface stress. It represents an unbalanced in-plane force per unit length distributed over boundary layers and drastically converges to zero toward central regions of each constituent. Furthermore, from Eq. (20), the impact of violating the equilibrium condition on the elastic tensor is obvious. Compared with the elastic constants of an ideal bulk lattice, $c_{\alpha\beta\mu\nu}$ is modified by an additional term, i.e., the last summation in Eq. (20), to provide an accurate description of the elastic modulus tensor, which commonly applies to both surface and interface regions.[26]

V. NUMERICAL RESULTS

In the preceding sections, we developed an analytical model which describes the determination of interface energy, interface stress, and interface elastic constant tensor in terms of EAM or TB-SMA potential functions. Although the model is derived for crystal-crystal interfaces, it is equally valid for monocrystalline surfaces.[15,24] In this section, we first calculate surface energy, surface stress, and surface elastic constants of freestanding metal films. Our model is then validated by comparing them with other atomistic simulations of the surface variables previously reported in literature.[14] Next, we present the calculations of interface material properties for various metal-metal bilayers.

A. Elastic properties of crystalline surfaces

The procedure to calculate surface variables is summarized by the following three parts: (a) preparing a freestanding metal film with a given initial atomic arrangement; (b) relaxing the system toward the minimum potential-energy configuration with zero applied strain; (c) recording values of γ, $f_{\alpha\beta}$, and $c_{\alpha\beta\mu\nu}$ under both unrelaxed and relaxed conditions.

The creation of a freestanding film sample is straightforward. A simulation cell is constructed with each atom residing at the position consistent with a perfect monocrystal without any deformation. Equivalently, the sample can also be obtained by confining an infinite lattice with two parallel planes separated by a finite distance. Periodic boundary conditions are then assumed along the two in-plane principal directions x_1 and x_2 of the cubic lattice while the dimension along the normal direction x_3 is finite to represent two (top and bottom) free surfaces. Because the film sample consists of atoms of a single species, the number of unit cells along x_1 and x_2 directions within the simulation cell can be chosen arbitrarily. The simulation results are insensitive to this option. The important parameter is the thickness of the slab. All film samples in this paper were chosen to have a thickness larger than 4 nm in order to prevent any interaction between the top and the bottom free surfaces. Due to the absence of constraint in the direction normal to the free surfaces, relaxations occur along x_3 axis, which then results in a variation in the interplanar spacing, usually distributed over several layers in the vicinity of the free surfaces. The atomic structure of each layer remains fixed and no in-plane adjustment is permitted because of the periodic boundary conditions prescribed on the side surfaces of the sample, i.e., surfaces normal to the x_1 and x_2 directions. Therefore, atoms tend to relax along the x_3 direction only, collectively layer by layer.

We used the large-scale atomic/molecular massively parallel simulator (LAMMPS)[27,28] into which the Hessian-free truncated Newton method[29] is implemented as the energy minimizer. The interatomic potentials employed were linked with the LAMMPS program under the parallel environment of message-passing interface. A final configuration was obtained so as to minimize the magnitudes of each force component acting on all particles. No single component of the atomic force was greater than 6.95×10^{-16} N$(=4\times10^{-7}$ eV/Å) in the final configuration. Once the final state was achieved, the surface variables were computed based on the analytical formulas, as given in Eqs. (18)–(20).

Following the above procedure, the surface energies, surface stress tensors, and surface elastic modulus tensors were calculated for (110) and (001) surfaces of ten bcc metals, and for (001) and (111) surfaces of six fcc metals. The results are listed in Tables I–IV, respectively. In all of these cases, the simulation supercell contains 10×10 unit cells along the x_1 and x_2 axes, and a finite thickness slightly larger than 4 nm along the x_3 direction. The values of γ, $f_{\alpha\beta}$, and $c_{\alpha\beta\mu\nu}$ were calculated for both relaxed and unrelaxed configurations. Surface energies do not change much upon relaxation [at most, 6.9% reduction for the case of Au (001) surface]. The relaxation effect is not really significant, compared with other uncertainties such as the selection of different types of interatomic potentials of which the effects will be discussed later in this section.

Surface stresses, however, strongly depend on the vertical (interlayer) relaxation effects. In most cases, except for Cr, Mo, W, and Fe (001) surfaces, relaxations result in considerable decreases of surface stress, as shown in the tables. Major difference in surface stresses before and after relaxation is found from their distributions through the thickness of film. In unrelaxed configurations, the distributions of surface stress are totally determined by the cutoff range introduced by a given interatomic potential function. For example, the surface stress distribution extends up to the first two layers for bcc (001) surfaces (Table II). However, it is localized only to the first layer for bcc (110) (Table I) because the cutoff distance of the potential used is shorter than the interlayer distance between two bcc (110) planes. In contrast, surface stresses in relaxed configurations are usually distributed over a larger range of interlayer distance. In the examples listed in Table II, contributions to f_{11} and f_{22} are made by about the first ten planes from the free surface, although the first two layers are still dominant.

We also investigated the relaxation effect on the surface elastic modulus tensor. Due to the symmetric properties of $c_{\alpha\beta\mu\nu}$ mentioned in the previous section, it is convenient to express $c_{\alpha\beta\mu\nu}$ by a 2×2 matrix with the subscripts relabeled as

TABLE I. Surface energy γ, surface stress $f_{\alpha\beta}$, and surface modulus $c_{\alpha\beta\mu\nu}$ of the (110) free surface calculated for bcc metals using the Johnson-Oh EAM potential (Ref. 23) (Li, Na, K and the upper rows of V, Nb, Ta, Mo, W, Fe) and the Finnis-Sinclair potential (Ref. 24) (Cr and the lower rows of V, Nb, Ta, Mo, W, Fe). Only nontrivial components of $f_{\alpha\beta}$ and $c_{\alpha\beta\mu\nu}$ are shown. The subscripts "1" and "2" denote the [001] and $[\bar{1}10]$ directions, respectively. "U" represents unrelaxed values and "R" stands for results after energy minimization. All entries are in units of J/m^2.

	γ		f_{11}		f_{22}		c_{11}		c_{12}		c_{21}		c_{22}		c_{33}	
Element	U	R	U	R	U	R	U	R	U	R	U	R	U	R	U	R
Li	0.23	0.23	0.13	0.10	0.32	0.24	−0.73	−0.35	−0.31	−0.25	−0.51	−0.39	−1.11	−0.81	0.04	−0.02
Na	0.16	0.16	0.07	0.05	0.18	0.13	−0.52	−0.28	−0.21	−0.15	−0.32	−0.23	−0.72	−0.52	−0.04	−0.07
K	0.10	0.10	0.05	0.03	0.11	0.07	−0.34	−0.19	−0.14	−0.09	−0.20	−0.14	−0.45	−0.31	−0.06	−0.06
V	1.63	1.61	1.51	0.49	2.69	1.77	−14.14	−11.36	−4.44	−2.15	−5.62	−3.43	−10.68	−5.52	−3.01	−2.40
	1.49	1.47	1.29	0.26	2.85	1.93	−10.00	−7.68	−1.69	−1.06	−3.25	−2.74	−7.43	−6.89	0.73	0.37
Nb	1.84	1.79	2.50	0.76	3.43	1.96	−18.03	−13.65	−6.76	−2.47	−7.69	−3.66	−13.73	−4.20	−4.98	−3.30
	1.71	1.66	2.19	0.30	3.66	2.16	−12.35	−9.12	−2.72	−1.77	−4.19	−3.64	−9.48	−8.98	0.53	0.26
Ta	1.97	1.94	1.46	0.57	3.47	2.44	−15.73	−12.06	−4.72	−2.81	−6.74	−4.68	−14.29	−9.58	−2.74	−2.61
	2.00	1.97	1.23	0.39	3.56	2.53	−10.99	−8.31	−1.72	−1.18	−4.05	−3.33	−10.57	−9.07	1.14	0.56
Cr	1.63	1.63	−0.73	−0.82	0.94	0.86	−11.93	−12.94	1.91	1.99	0.23	0.29	−2.64	−2.15	2.18	2.10
Mo	2.20	2.19	−0.37	−0.98	3.28	2.75	−22.99	−21.70	−1.90	−0.94	−5.55	−4.68	−12.95	−10.17	−0.97	−1.12
	1.83	1.82	1.37	0.77	2.59	2.01	−20.42	−26.83	−1.77	−1.24	−2.99	−2.49	−9.73	−5.94	0.97	0.53
W	2.77	2.76	−1.06	−1.57	3.68	3.17	−24.13	−22.68	−0.93	−0.22	−5.69	−4.96	−14.97	−12.62	0.11	−0.20
	2.58	2.57	0.75	0.27	2.95	2.38	−21.14	−25.99	−1.18	−0.72	−3.37	−2.83	−12.18	−8.71	1.51	1.03
Fe	1.52	1.51	−0.52	−0.67	1.88	1.58	−7.66	−6.45	−0.36	−0.14	−2.78	−2.40	−8.62	−7.52	0.38	0.14
	1.70	1.70	−0.93	−1.05	1.87	1.61	−3.84	−3.02	2.11	2.12	−0.69	−0.54	−4.62	−4.26	2.97	2.68

$$1 = 11, \quad 2 = 22, \quad 3 = 12, \tag{21}$$

as given in the tables. From the simulation results, it is observed that $c_{\alpha\beta\mu\nu}$ demonstrates larger dependence on the relaxation of atomic positions than $f_{\alpha\beta}$. In several cases, the relaxation even changes the sign of $c_{\alpha\beta\mu\nu}$, which is not the case for surface stresses. As illustrated in Tables I–IV, most surface modulus components are negative, which implies that in general surface stress values decrease as applied elastic strains increase. This observation apparently contradicts the corresponding constitutive relationship drawn from the classical theory of elasticity, which agrees well with recent reports.[12,14]

The bcc (110) surfaces (Table I) are orthotropic and thus possess only a twofold in-plane rotational symmetry, in addition to the mirror-imaged symmetries with respect to the two planes which are perpendicular to the surface. Among the two components of principal surface stress, the one of the close-packed direction [001] is smaller than the other one associated with the loose-packed direction $[\bar{1}10]$. In particular, Cr, Mo, W, and Fe (110) surfaces reveal the negative principal stress along the close-packed direction [001]. The elastic constants obey the relationships $c_{1111} \neq c_{2222}$ and $c_{1122} \neq c_{2211}$ due to the loss of symmetry between the first and second pairs of indices. On the other hand, bcc (001), fcc (001), and fcc (111) surfaces are isotropic since they fulfill the rotational symmetry higher than threefold.[20] On these surfaces, both the surface stress and the surface elastic modulus can be represented by the most general expressions with the second- and fourth-order isotropic tensors as

$$f_{\alpha\beta} = \Gamma \delta_{\alpha\beta}, \quad c_{\alpha\beta\mu\nu} = \Gamma \delta_{\alpha\beta}\delta_{\mu\nu} + \Lambda \delta_{\alpha\mu}\delta_{\beta\nu} + \Sigma \delta_{\alpha\nu}\delta_{\beta\mu}, \tag{22}$$

where Γ, Λ, and Σ are scalars. Therefore, we only need one component to represent $f_{\alpha\beta}$ and three independent components for $c_{\alpha\beta\mu\nu}$, as provided in Tables II–IV.

As pointed out by Gumbsch and Daw[15] and Streitz *et al.*,[16] the calculated results of surface and interface properties, to some extent, depend on the selection of interatomic potentials. To examine this effect for bcc crystals, we compared two potentials, i.e., the EAM potential derived by Johnson and Oh[23] and the Finnis-Sinclair potential based on the second-moment approximation to tight-binding theory.[24] We considered two free surfaces, (110) and (001), and six bcc elements, V, Nb, Ta, Mo, W, and Fe, as given in Tables I and II. While surface elastic constants for these bcc crystals are not available elsewhere, the calculations of surface energy and surface stress of V, Nb, Ta, Mo, and W by the Finnis–Sinclair model have already been performed,[11] and our current results are in perfect agreement. For each of the

TABLE II. Surface energy γ, surface stress $f_{\alpha\beta}$, and surface modulus $c_{\alpha\beta\mu\nu}$ of the (001) free surface calculated for bcc metals using the Johnson-Oh EAM potential (Ref. 23) (Li, Na, K and the upper rows of V, Nb, Ta, Mo, W, Fe) and the Finnis-Sinclair potential (Ref. 24) (Cr and the lower rows of V, Nb, Ta, Mo, W, Fe). Only nontrivial components of $f_{\alpha\beta}$ and $c_{\alpha\beta\mu\nu}$ are shown. The subscripts "1" and "2" denote the [100] and [010] directions, respectively. "U" represents unrelaxed values and "R" stands for results after energy minimization. All entries are in units of J/m^2.

	γ		$f_{11}=f_{22}$		$c_{11}=c_{22}$		$c_{12}=c_{21}$		c_{33}	
Element	U	R	U	R	U	R	U	R	U	R
Li	0.27	0.27	0.36	0.26	−1.49	−1.14	−1.29	−0.88	−0.60	−0.41
Na	0.18	0.18	0.21	0.14	−1.00	−0.75	−0.81	−0.54	−0.39	−0.29
K	0.11	0.11	0.12	0.08	−0.63	−0.45	−0.49	−0.31	−0.24	−0.17
V	1.88	1.84	3.12	1.99	−15.31	−7.57	−11.00	−4.39	−4.35	−1.36
	1.76	1.73	3.47	2.42	−11.44	−10.49	−7.10	−6.99	−1.35	−2.26
Nb	2.14	2.04	3.96	1.89	−19.85	−2.30	−13.49	1.17	−4.74	2.23
	2.04	1.95	4.47	2.53	−14.85	−13.49	−7.52	−9.45	−0.22	−3.20
Ta	2.29	2.27	4.04	2.93	−20.29	−14.81	−15.59	−10.56	−7.28	−5.25
	2.34	2.32	4.33	3.24	−15.98	−14.15	−11.53	−9.95	−4.26	−4.05
Cr	1.78	1.77	1.21	1.51	−4.63	−6.82	−7.31	−9.83	−5.25	−7.24
Mo	2.48	2.48	3.97	4.11	−18.28	−17.31	−16.00	−14.95	−7.99	−6.52
	2.11	2.09	3.02	2.24	−14.36	−8.78	−11.77	−5.91	−6.69	−2.14
W	3.12	3.10	4.48	4.97	−20.92	−20.52	−19.57	−19.31	−10.73	−9.32
	2.92	2.92	3.46	3.03	−17.65	−14.91	−16.30	−13.28	−10.24	−8.00
Fe	1.72	1.72	2.27	2.54	−11.96	−12.46	−11.53	−12.20	−7.11	−7.17
	1.92	1.90	2.38	2.84	−7.32	−8.03	−9.33	−10.48	−5.59	−6.08

six atomic species (double rows in Tables I and II), the upper row is for the results by the Johnson-Oh EAM potential while the lower row is for those by the Finnis-Sinclair potential. Within reasonable margins, the two potentials agree in surface energy values γ. In the relaxed case, the maximal difference between them is 16.89%, corresponding to Mo (110) surface. However, larger disagreements are found in surface stresses $f_{\alpha\beta}$. In (110) surface cases, f_{11} reveals a larger discrepancy than f_{22}. In particular, Mo and W even result in opposite signs of f_{11} values between the two interatomic potentials. Generally speaking, we observe that computed results of surface elastic constants for bcc (001) surfaces are less potential dependent than those for (110) surfaces of the same species.

We further studied the potential dependence of surface properties for the six fcc species and the results are listed in Tables III and IV. We used the Johnson's fcc alloy EAM potential,[21] but modified it slightly in order to include up to fifth nearest neighbors. Our results are given in the corresponding upper rows in the tables. We also present in the lower rows the results from Shenoy,[14] which were based on the EAM potential developed by Oh and Johnson.[30] These EAM-type interatomic potentials, as well as those for bcc crystals, share the same functional forms, as displayed in Eqs. (15) and (16), and common schemes for fitting parameters with experimental data. As in the cases of bcc crystals, the surface energy values reveal the least dependence on the potential employed, for both fcc (001) and (111) surfaces. Results of surface stresses are also in good agreement between the potentials, except for the Ni (111) surface where the signs do not agree. On the other hand, the two EAM potential functions show rather significant difference in the values of surface elastic constants $c_{\alpha\beta\mu\nu}$. In several cases, such as c_{1122} on Cu, Ag, and Pd (001) surfaces, the signs of surface elastic constants do not agree. However, most of the surface elastic constants remain within the comparable order even though the potential function is changed. This confirms the view, addressed in Ref. 15, that "qualitative conclusions rather than precise numerical results" can still be expected even for the surface elastic constants. In addition to the difference of the empirical potentials employed, the computational schemes are also different between our results and those of Shenoy[14] in Tables III and IV. We used the analytical formulas we derived under zero strain state while Shenoy[14] used the incremental approach by applying a series of strains values. From our experience, this difference in schemes is not as significant as the difference in the selection of empirical potentials.

The potential-induced discrepancy of the calculated values of surface stresses and surface elastic constants is perhaps an inherent attribute of empirical interatomic potentials, because they were primarily fitted to provide an accurate

TABLE III. Surface energy γ, surface stress $f_{\alpha\beta}$, and surface modulus $c_{\alpha\beta\mu\nu}$ of the (001) free surface calculated for fcc metals using the Johnson EAM potential (Ref. 21) (the upper rows). The lower rows for each atomic species are the results from Shenoy (Ref. 14). Only nontrivial components of $f_{\alpha\beta}$ and $c_{\alpha\beta\mu\nu}$ are shown. The subscripts "1" and "2" denote the [100] and [010] directions, respectively. "U" represents unrelaxed values and "R" stands for results after energy minimization. All entries are in units of J/m^2.

	γ		$f_{11}=f_{22}$		$c_{11}=c_{22}$		$c_{12}=c_{21}$		c_{33}	
Element	U	R	U	R	U	R	U	R	U	R
Cu	1.23	1.22	1.89	1.41	−8.93	−6.32	−1.12	−0.57	−1.26	−1.34
		1.32		1.03		−4.16		4.30		−1.00
Ag	0.86	0.85	1.77	1.13	−10.09	−6.27	−4.27	−2.94	−1.49	−1.48
		0.86		0.89		−3.46		1.90		−1.68
Au	0.87	0.81	3.52	1.49	−19.09	−7.10	−12.14	−5.67	−4.52	−3.17
		0.79		1.40		−5.27		−2.53		−3.95
Ni	1.56	1.56	1.51	1.37	−7.05	−6.23	4.72	4.72	−0.87	−0.93
		1.53		0.70		−4.87		9.50		0.19
Pd	1.40	1.37	3.40	1.98	−20.99	−12.13	−11.54	−7.70	−3.01	−2.83
		1.29		1.68		−6.44		0.09		−3.70
Pt	1.55	1.48	5.16	2.52	−29.40	−13.25	−16.89	−9.30	−6.46	−5.12
		1.40		2.28		−8.89		−2.83		−6.23

description of a bulk lattice. It is not our purpose here to provide a detailed discussion of the accuracy of EAM potentials. Nevertheless, it is perhaps necessary to mention that EAM potentials are still very useful, particularly for the large-scale computational of noncoherent interfaces. In order to keep periodic boundary conditions on the sides of a bicrystal specimen, we have to minimize the undesired mismatch effect due to the size difference of each single crystal specimen originated from the difference in lattice parameters. This argument typically requires us to employ large-scale computation containing as many as over a million atoms. Details will be presented in the next section.

TABLE IV. Surface energy γ, surface stress $f_{\alpha\beta}$, and surface modulus $c_{\alpha\beta\mu\nu}$ of the (111) free surface calculated for fcc metals using the Johnson EAM potential (Ref. 21) (the upper rows). The lower rows for each atomic species are the results from Shenoy (Ref. 14). Only nontrivial components of $f_{\alpha\beta}$ and $c_{\alpha\beta\mu\nu}$ are shown. The subscripts "1" and "2" denote the $[1\bar{1}0]$ and $[11\bar{2}]$ directions, respectively. "U" represents unrelaxed values and "R" stands for results after energy minimization. All entries are in units of J/m^2.

	γ		$f_{11}=f_{22}$		$c_{11}=c_{22}$		$c_{12}=c_{21}$		c_{33}	
Element	U	R	U	R	U	R	U	R	U	R
Cu	1.13	1.12	1.27	0.95	−2.49	−1.60	1.20	1.49	−1.21	−1.06
		1.24		0.54		−1.97		−2.24		0.14
Ag	0.78	0.77	1.37	0.95	−5.59	−3.99	−1.89	−1.12	−1.16	−0.95
		0.79		0.64		−3.00		−2.05		−0.49
Au	0.74	0.70	3.09	1.67	−14.70	−8.16	−6.28	−3.07	−2.66	−1.70
		0.69		1.64		−7.97		−2.70		−2.62
Ni	1.43	1.43	0.68	0.54	3.21	3.43	6.49	6.43	−1.29	−1.22
		1.43		−0.11		2.17		−1.36		1.77
Pd	1.25	1.23	2.79	1.85	−14.06	−9.83	−6.92	−4.58	−2.16	−1.69
		1.16		1.63		−7.81		−3.79		−2.00
Pt	1.34	1.30	4.40	2.65	−20.78	−12.86	−8.35	−4.54	−4.01	−2.83
		1.23		2.53		−12.67		−4.90		−3.89

B. Elastic properties of metal-metal interfaces

Following the similar procedure as outlined above, we calculated the interface energy, the interface stress tensor, and most importantly, the interface modulus tensor for several fcc-fcc (001) and (111) parallel-oriented noncoherent bicrystalline systems. All the results presented in this section were obtained by employing the Johnson fcc alloy potential,[21] with minor modification in order to span the interatomic interaction distance up to fifth nearest neighbors. Unlike surface cases, alloy potentials have been adopted primarily for the calculations of interface properties in previous studies.[15,16] In dealing with multiple crystal constituents, alloy potentials are preferred because it is more likely that an energetically favorable interface structure can be found by an iterative energy minimizer.

For atomistic calculations of noncoherent interfaces, several additional issues need to be addressed. First of all, a bicrystal simulation cell (a box), with periodic boundary conditions on the plane normal to the interface, must be carefully constructed due to the difference of lattice parameters between the two crystals. The top and bottom boundaries of the periodic cell are free to, respectively, represent free surfaces of each constituent crystal. The separation distance between the two components across the interface does not seem to be relevant to simulation results since the bicrystalline system would relax toward the same final atomic configuration from any reasonable choice of initial separation. For the purpose of simplicity and convenience, we take an average value for the lattice constants of both crystals for the parameter of interfacial distance (before relaxation), in all of our interface calculations. Similar to surface calculations, the thickness of each phase in the periodic cell is selected to be larger than 4 nm for all systems to avoid any noticeable interaction among the interface and the two free surfaces. As a result, the thickness of the supercell along the x_3 direction is more than 8 nm, containing approximately 24 unit cells for fcc-fcc (001) systems and 40 cells for (111) ones. After all, the most difficult task in the construction of periodic supercell lies in the selection of the in-plane number of unit cells for each phase of the bilayers, as described as follows.

We prepare two single crystal thin film specimens: one has $m \times m$ in-plane number of unit cells and the other has $n \times n$. The total in-plane sizes of each specimen are thus $ma \times ma$ and $nb \times nb$, where a and b are lattice parameters of each crystal. We put them together to form a planar interface model and consequently make one huge supercell for simulations. Because of the difference in lattice parameters (a and b), there is a mismatch in the side lengths between the two specimens (i.e., $ma \neq nb$). By searching for the best combination of m and n with given a and b, we can minimize this mismatch length (i.e., $|ma-nb|$) between the two crystal samples. Once m and n are determined, we stretch the smaller specimen a little in order to perfectly match both specimen at their side boundaries. This process enables us to impose a periodic boundary condition commonly on both specimens. The whole model finally becomes a periodic supercell that has a perfect in-plane periodic boundary condition.

The strain we applied to the smaller specimen can be quantified by a residual interface misfit strain[16] as

$$\epsilon_m = \frac{ma - nb}{(ma + nb)/2}, \tag{23}$$

which reflects the mismatch of the two single crystal simulation boxes in a supercell and should not be read as the conventional misfit strain in a thin film, $\varepsilon=(a-b)/a$, at the level of two unit cells. For most material combinations, the small residual mismatch strain, Eq. (23), must be reconciled by elastically deforming one crystal along periodic dimensions to match the other phase as described above. The m/n ratios and the corresponding ϵ_m used are listed in Tables V and VI for several fcc-fcc bilayered systems. In all cases, we limited the residual misfit strain $\epsilon_m \leqslant 0.05\%$, where the periodic cells typically consist of several hundred thousand atoms to million sizes. As a result, its effect is negligible. The most idealized systems with zero misfit strains are Au/Ni and Pt/Ni, benefited from the corresponding lattice constants adopted in Johnson fcc alloy EAM potential.[21] Further reduction of ϵ_m can also be attempted by increasing the number of unit cells substantially (by an order). This requires much higher computational cost while the simulation results are insensitive, since ϵ_m is already small enough with the magnitude of one part in ten thousand. An example of typical simulation models is shown in Fig. 2 for which an atomistic configuration viewer, AtomEye,[31] is used.

Tables V and VI present the interface energy σ, interface stresses $h_{\alpha\beta}$, and interface elastic constants $c_{\alpha\beta\mu\nu}$ for several isotropic fcc (001) and (111) parallel-oriented interfaces. Compared with surface energies, the excess energies on (001) interfaces are strongly influenced by the vertical relaxation process. This is somewhat due to the arbitrary selection of the initial (i.e., before relaxation) separation distance across the interface. However, such large relaxation effects are not found on close-packed (111) interfaces. The common characteristics on both interface orientations are that interface energies decrease upon relaxation while the corresponding interface stresses tend to increase for all systems except the Pt/Ni (111) interface. Consistent with fcc surfaces, the excess energies and stresses on (111) interfaces are found to be smaller than those on (001), except for interface stresses of Pt/Ni and Pt/Cu systems. In particular, the interface stress of Pt/Ni system deviates significantly from this tendency. The relatively less accurate representation of EAM potentials for the nickel system may be responsible for these discrepancies since even negative interface energies and/or interface stresses have been found in previous studies involving Au/Ni and Pt/Ni systems.[15,16]

Interface energies and stresses are generally in quantitative agreement with the values computed by Gumbsch and Daw,[15] as summarized in Tables V and VI, although they used another type of EAM potential and smaller sizes of atomic models. The only exception of note is that we do not have any negative value of interface stresses (after relaxation) while a few negative values were reported in Ref. 15. We again emphasize that no systematic computation of interface elastic constants can be found elsewhere and thus the values in Tables V and VI are, to the best of our knowledge, the first atomistic calculation results ever.

TABLE V. Interface energy σ, interface stress $h_{\alpha\beta}$, and interface modulus $c_{\alpha\beta\mu\nu}$ calculated for several (001) parallel-oriented fcc-fcc bicrystals using the Johnson EAM potential (Ref. 21). (Pd/Cu, Pt/Cu, and the upper rows for Ag/Ni, Au/Ni, Ag/Cu, Au/Cu, and Pt/Ni). The lower rows for Ag/Ni, Au/Ni, Ag/Cu, Au/Cu, and Pt/Ni are the results from Gumbsch and Daw (Ref. 15). Only nontrivial components of $h_{\alpha\beta}$ and $c_{\alpha\beta\mu\nu}$ are shown. The subscripts "1" and "2" denote the [100] and [010] directions, respectively. "U" represents unrelaxed values and "R" stands for results after energy minimization. All entries are in units of J/m^2.

		σ		$h_{11}=h_{22}$		$c_{11}=c_{22}$		$c_{12}=c_{21}$		c_{33}	
Element	$m/n(\epsilon_m)$	U	R	U	R	U	R	U	R	U	R
Ag/Ni	37/43 (0.020%)	5.26	0.94	−5.51	1.20	1.04	−11.11	10.78	3.28	3.93	2.14
	6/7 (0.407%)		0.82		0.83						
Au/Ni	44/51 (0.000%)	4.01	0.64	−5.87	0.70	−0.77	−10.78	8.54	2.40	6.25	3.35
	6/7 (0.651%)		0.54		0.71						
Ag/Cu	38/43 (0.016%)	3.04	0.59	−3.09	0.82	−3.45	−7.57	4.32	0.52	3.23	2.00
	7/8 (1.008%)		0.47		0.53						
Au/Cu	31/35 (0.036%)	2.46	0.35	−3.55	0.34	−4.89	−6.53	2.28	0.32	4.53	2.82
	7/8 (1.253%)		0.29		0.33						
Pt/Ni	44/49 (0.000%)	4.39	0.49	−4.00	0.34	−16.73	−9.34	−1.61	1.98	4.82	4.94
	9/10 (0.227%)		0.32		0.04						
Pd/Cu	66/71 (0.029%)	2.70	0.44	−2.52	0.33	−8.67	−4.99	1.94	0.90	3.76	2.65
Pt/Cu	59/64 (0.035%)	3.07	0.30	−2.28	0.47	−17.03	−4.96	−4.60	−2.41	3.16	1.35

Figure 3 shows the calculated stress variation across a 40-layer (111) Au/Ni bicrystal thin film. We depict the layer-by-layer contributions to the interface (surface) stress by plotting the lateral stress acting on individual layers averaged by the total interface (surface) area, at both zero-strain state and the equilibrium configuration. In the former case, the system is only relaxed by adjusting the interplanar separation distances for a minimum potential energy, while the in-plane

TABLE VI. Interface energy σ, interface stress $h_{\alpha\beta}$, and interface modulus $c_{\alpha\beta\mu\nu}$ calculated for several (111) parallel-oriented fcc-fcc bicrystals using the Johnson EAM potential (Ref. 21). (Pd/Cu, Pt/Cu, and the upper rows for Ag/Ni, Au/Ni, Ag/Cu, Au/Cu, and Pt/Ni). The lower rows for Ag/Ni, Au/Ni, Ag/Cu, Au/Cu, and Pt/Ni are the results from Gumbsch and Daw (Ref. 15). Only nontrivial components of $h_{\alpha\beta}$ and $c_{\alpha\beta\mu\nu}$ are shown. The subscripts "1" and "2" denote the $[1\bar{1}0]$ and $[11\bar{2}]$ directions, respectively. "U" represents unrelaxed values and "R" stands for results after energy minimization. All entries are in units of J/m^2.

		σ		$h_{11}=h_{22}$		$c_{11}=c_{22}$		$c_{12}=c_{21}$		c_{33}	
Element	$m/n(\epsilon_m)$	U	R	U	R	U	R	U	R	U	R
Ag/Ni	37/43 (0.020%)	0.97	0.58	−0.67	0.40	2.48	0.74	2.08	2.22	−0.13	−0.53
	6/7 (0.407%)		0.42		0.32						
Au/Ni	44/51 (0.000%)	0.51	0.28	−0.50	0.20	0.16	−0.30	−0.71	0.25	0.18	−0.17
	6/7 (0.651%)		0.14		−0.08						
Ag/Cu	38/43 (0.016%)	0.56	0.31	−0.09	0.43	−0.94	−1.46	−0.85	−0.42	−0.08	−0.30
	6/7 (1.008%)		0.24		0.32						
Au/Cu	31/35 (0.036%)	0.26	0.08	0.05	0.20	−3.01	−1.64	−2.98	−1.36	0.01	−0.03
	6/7 (1.253%)		0.00		0.01						
Pt/Ni	44/49 (0.000%)	0.43	0.04	1.01	0.62	−9.84	−4.12	−7.33	−3.12	−0.74	−0.18
	6/7 (0.227%)		−0.12		−0.57						
Pd/Cu	66/71 (0.029%)	0.48	0.17	0.22	0.26	−3.52	−1.19	−2.95	−0.93	−0.17	0.00
Pt/Cu	59/64 (0.035%)	0.35	0.00	1.14	0.54	−10.09	−3.52	−7.24	−2.79	−0.87	−0.09

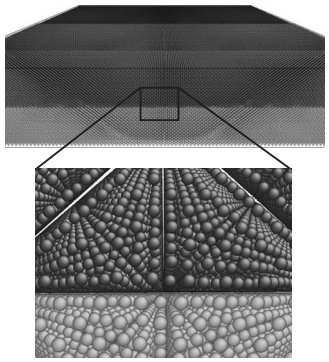

FIG. 2. A perspective view of the simulation model for Ag/Ni bicrystal of 1 246 532 atoms. The number of unit cells is 105 $\times$105$\times$12 for Ag and 122$\times$122$\times$12 for Ni. The size of the simulation box is 429.45$\times$429.45$\times$49.08 Å^3 for Ag part and 429.44 $\times$429.44$\times$42.24 Å^3 for Ni part, which needs the negligible amount of 0.002% misfit strain for periodic boundary condition imposed commonly on both zones.

structure remains the same as bulk values. The significant contributions to the surface and interface stresses come from the first three layers adjacent to the free surfaces and the interface. The stresses essentially decay to zero at the central regions of each constituent. Obviously, a positive net stress exists if a summation is performed over the contributions from each layer. For most metal-metal bilayered structures, the two surface stresses and the interface stress are tensile, and they tend to compress the bulk regions to achieve an energetically more stable state. The curve symbolized with △ in Fig. 3 represents such an equilibrium configuration achieved after an additional isotropic in-plane relaxation. Under this state, the sum of stresses over all layers vanishes, because the tensile surface and interface stresses are balanced by the compressive bulk stresses slightly deviated

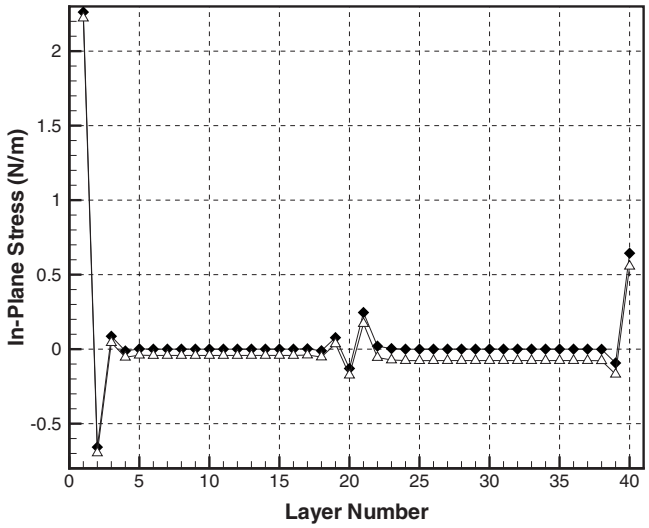

FIG. 3. The distribution of in-plane stress at each layer through the thickness for the Au/Ni (111) bicrystal at zerostrain (◆) and at equilibrium states under biaxial strains (△). Detailed description is given in the text.

from zero. In this equilibrated system, the excess nature of surface and interface properties requires that σ, $h_{\alpha\beta}$, and $c_{\alpha\beta\mu\nu}$ must be determined in reference to the central layers of each constituent crystal.

Interfacial thermodynamic variables are localized within a few in-depth layers from the interface. For example, the six central layers (layers 18–23) contribute above 95% to the Au/Ni interface elastic constants, which implies three layers in each constituent. This notion is comparable with the surface properties as three layers are needed for Au or Ni free surface variables on the same accuracy. On the other hand, from Tables I–VI, we have also found that the interface elastic constants are only slightly smaller than those of surfaces with the same orientations, although σ and $h_{\alpha\beta}$ are roughly 50% lower than γ and $f_{\alpha\beta}$. These observations imply that the interface stress effects are equally important to those of free surfaces in practical applications. This will be clarified in our future study through examples of continuum micromechanics incorporating the values of interface elastic constants reported in this paper.

VI. CONCLUDING REMARKS

We have presented an analytical formulation and computer implementation of interface elastic properties in conjunction with EAM-type interatomic potential functions, with particular emphasis on the determination of interface elastic moduli tensors. The model was applied to a series of bcc and fcc free surfaces, and validated by comparing the results with similar atomistic simulations available in the literature. We have then presented the calculation of interface energy, interface stress tensor, and the interface elastic tensor for several metal-metal bicrystalline interfaces. In most cases, reasonable agreement has been observed in comparison with previously reported values of interface energies and interface stresses.[14–16] The calculated results of interface material properties can find immediate applications in the continuum micromechanical studies incorporating surface and/or interface elasticity and relevant size effects.[4–6] This applicability has served as the main motivation of the present study because such quantities are indispensable for the completion of the theoretical framework of surface and/or interface nanomechanics. In the following, we summarize a few important observations:

(i) Surface and interface relaxations, due to the loss of constraint along the direction normal to crystalline boundaries, are found to play a significant role in most surface and interface material constants, especially in certain components of surface and/or interface stress and modulus tensor.

(ii) The magnitudes of surface and interface elastic constants depend on crystalline orientations. These material constants are generally smaller in close-packed surfaces and interfaces, i.e., bcc (110) and fcc (111), than those in less close-packed systems, e.g., (001).

(iii) The excess energies and stresses of bicrystal interfaces are smaller than those in free surfaces with the same crystal orientations. However, such a trend is less obvious for the excess elastic constants. We have not observed any negative values of interface stresses in contrast to previous results of Ref. 15.

(iv) The atomistic determinations of surface and interface material properties are generally based on the differentiation of potential energy with respect to elastic strains, either performed analytically or numerically through finite difference schemes. These two approaches almost make no difference in surface calculations. However, the proposed analytical formulation shows much greater promise in the case of noncoherent interface simulations, due to the expensive computational cost inherently associated with large size of supercell accommodating periodic boundary conditions. In other words, the current theoretical model enables us to extract all the interface material properties of interest from a single strain state, i.e., an atomic configuration under zero strain.

Referring to Gibbs' dividing surface separating two homogeneous single crystals, there are generally two types of interface stresses studied in the literature.[4,18,32] One is associated with the simultaneous deformation of both phases along the interface and the other corresponds to the in-plane strain of one phase relative to the other. Gurtin *et al.*[32] studied the most general case and additionally introduced a third type of interface stress to measure the change in interfacial energy due to stretch. This paper, as well as previous atomic simulations of interface stresses,[15,16] has contributed to measuring the first type of interface stress because the interfacial structure is assumed to remain unchanged (stable). The second and third types of interface stresses have no contribution in this case. Additional terms and extra elastic constants in constitutive equations, which are associated with the second and the third types, will be necessary when we account for structural changes and/or non-negligible relative strains. However, to our knowledge, no atomic simulation and experimental measurement have been reported yet for the second and third types of interface stresses and the corresponding interface elastic constants. Further studies are therefore needed to explore this topic in the future.

ACKNOWLEDGMENTS

S.J. is supported by the University of Wyoming. S.Y.K. acknowledges the support by the second stage of the Brain Korea 21 Project.

*Corresponding author. sjun@uwyo.edu

[1] J. D. Eshelby, Proc. R. Soc. London, Ser. A **241**, 376 (1957).
[2] T. Mura, *Micromechanics of Defects in Solids*, 2nd ed. (Springer, New York, 1987).
[3] S. Nemat-Nasser and M. Hori, *Micromechanics: Overall Properties of Heterogeneous Materials*, 2nd ed. (North Holland, Amsterdam, 1998).
[4] J. W. Cahn and F. Larché, Acta Metall. **30**, 51 (1982).
[5] P. Sharma, S. Ganti, and N. Bhate, Appl. Phys. Lett. **82**, 535 (2003).
[6] C. Mi and D. Kouris, J. Mech. Mater. Struct. **1**, 763 (2006).
[7] M. E. Gurtin and A. I. Murdoch, Arch. Ration. Mech. Anal. **59**, 389 (1975).
[8] M. E. Gurtin and A. I. Murdoch, Int. J. Solids Struct. **14**, 431 (1978).
[9] C.-W. Pao, D. J. Srolovitz, and C. V. Thompson, Phys. Rev. B **74**, 155437 (2006).
[10] C. W. Price and J. P. Hirth, Surf. Sci. **57**, 509 (1976).
[11] G. J. Ackland and M. W. Finnis, Philos. Mag. A **54**, 301 (1986).
[12] R. E. Miller and V. B. Shenoy, Nanotechnology **11**, 139 (2000).
[13] L. G. Zhou and H. Huang, Appl. Phys. Lett. **84**, 1940 (2004).
[14] V. B. Shenoy, Phys. Rev. B **71**, 094104 (2005).
[15] P. Gumbsch and M. S. Daw, Phys. Rev. B **44**, 3934 (1991).
[16] F. H. Streitz, R. C. Cammarata, and K. Sieradzki, Phys. Rev. B **49**, 10707 (1994).
[17] F. Liu, in *Handbook of Theoretical and Computational Nanotechnology*, edited by M. Rieth and W. Schommers (American Scientific, Stevenson Ranch, California, 2006), Vol. 4, Chap. 10, pp. 577–625.
[18] R. C. Cammarata, Prog. Surf. Sci. **46**, 1 (1994).
[19] H. Ibach, Surf. Sci. Rep. **29**, 195 (1997).
[20] M. J. Buerger, *Elementary Crystallography* (Wiley, New York, 1963), Chap. 11.
[21] R. A. Johnson, Phys. Rev. B **39**, 12554 (1989).
[22] R. A. Johnson, Phys. Rev. B **41**, 9717 (1990).
[23] R. A. Johnson and D. J. Oh, J. Mater. Res. **4**, 1195 (1989).
[24] M. W. Finnis and J. E. Sinclair, Philos. Mag. A **50**, 45 (1984); **53**, 161 (1986).
[25] R. A. Johnson, Phys. Rev. B **6**, 2094 (1972).
[26] M. S. Daw and M. I. Baskes, Phys. Rev. B **29**, 6443 (1984).
[27] S. J. Plimpton, J. Comput. Phys. **117**, 1 (1995).
[28] http://lammps.sandia.gov
[29] J. Nocedal and S. J. Wright, *Numerical Optimization* (Springer, New York, 1999), Chap. 6.
[30] D. J. Oh and R. A. Johnson, J. Mater. Res. **3**, 471 (1988).
[31] J. Li, Modell. Simul. Mater. Sci. Eng. **11**, 173 (2003).
[32] M. E. Gurtin, J. Weissmüller, and F. Larché, Philos. Mag. A **78**, 1093 (1998).